MEMOIRS OF THE SCHOOL OF ENGINEERING, OKAYAMA UNIVERSITY, Vol. 7, No. 2, OCTOBER 1972

Analysis on Magnetic Characteristics of Three-Phase Core-Type Transformers [Part II: Non-Linear Solutions and Experimental Results for R3-Type Core]

Takayoshi NAKATA*, Yoshiyuki ISHIHARA*, and Hideki MORIMOTO*

(Received September 16, 1972)

Synopsis

This paper deals with the magnetic characteristics (the flux distributions, core losses, etc.) of three-phase core-type transformers with double-layer. In the preceding report, only linear solutions have been given. In this paper, also non-linear solutions are discussed. Therefore, the flux waves of each magnetic path are distorted and contain various harmonics. When core losses are calculated, the hysteresis losses of minor loops are taken account. The results of analysis are compared with those of experiments.

It is concluded that the principal cause for increasing core losses of this type core is the eddy current loss produced by harmonic fluxes. The flux distributions and the core losses depend on the shapes of the magnetization curve and the core-loss curve, that is, on the quality of the materials.

1. INTRODUCTION

In the previous report(1), we have already reported the procedure analysing the magnetic circuits, the fundamental equations and the linear solutions of the cores which are presently used and consist of complicated magnetic circuits. In consideration of the non-linearity, we have analysed(2) the magnetic characteristics of the R6-type core which is composed of a triple-layer core and is used as a large power transformer core. And the experimental results have been compared with the results of analysis. This paper discribes the non-linear solutions and experimental results obtained from the R3-type core which comprises three independent magnetic paths and is usually used for a distribution transformer with wound cores as well as a middle power transformer.

The nomenclature of the type of cores, the normalizing method of the core dimensions, the symbols used in equations, the assumptions on simplicity of analysis and the expression of magnetization curves to conduct the numerical calculations are the same as the previous report(1).

---

* Department of Electrical Engineering

2. ANALYSIS OF MAGNETIC CIRCUITS

Figure 1(a) represents a double-layer core which is divided into three independent magnetic paths by ducts of the width δ. This construction is the main subject of this paper and is named the R3-type. Figure 1(b) shows the B-type core which is composed of simple magnetic circuit and will be compared with the characteristics of the R3-type core.

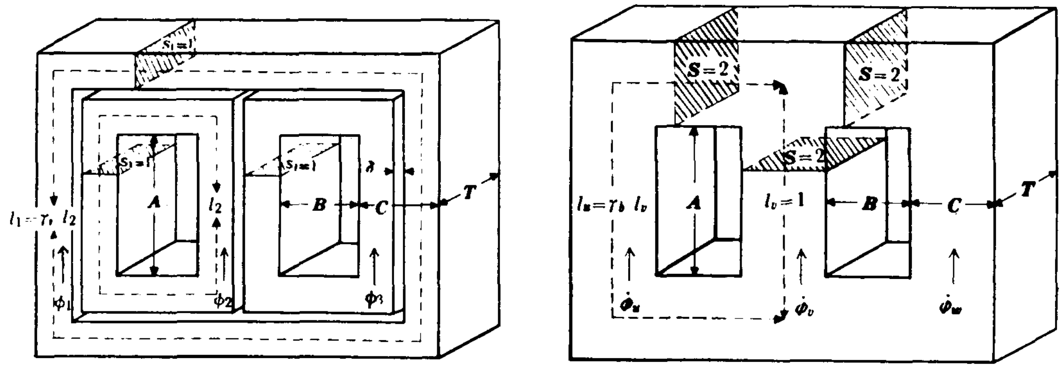

$\gamma_r = l_1/l_2$

(a) R3-type core

$\gamma_B = l_u/l_v$

(b) B-type core

Fig.1 Schematic diagrams of transformer-cores.

Figure 2 shows an electrical equivalent circuit of Fig.1(a). In the subsequent discussions, we represent the maximum values of respective quantities by capital letters, the instantaneous values by small letters and the branch names by subscripts.

Neglecting the width δ of ducts in Fig.1(a) and normalizing the cross-sectional area S_1 of the magnetic paths to 1, the following equations are satisfied between the fluxes ϕ_u and ϕ_w of the legs and the flux densities b_1, b_2 and b_3 in the magnetic paths.

$$b_2 = b_1 - \phi_u \ , \qquad (1)$$

$$b_3 = b_1 + \phi_w \ . \qquad (2)$$

The magnetomotive force m_1 impressed to the outer magnetic path is $m_u - m_w$. Similarly, we obtain the following equations.

$$m_1 = m_u - m_w \ ,$$

$$m_2 = m_v - m_u \ ,$$

$$m_3 = m_w - m_v \ .$$

Hence,

$$m_1 + m_2 + m_3 \equiv 0 \ . \qquad (3)$$

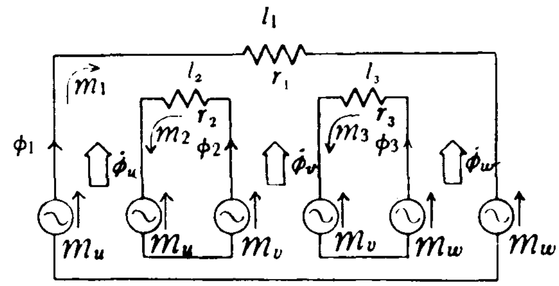

Fig.2 Equivalent circuit of R3-type core.

Magnetic field intensity h is generally a non-linear function of flux density b. Now let us represent the non-linear function by Eq.(4).

$$h=f(b). \tag{4}$$

We obtain the following equation from Eq.(3).

$$\gamma_r f(b_1)+f(b_2)+f(b_3)\equiv 0 \ , \tag{5}$$

where γ_r is a ratio of the mean path-length l_1 of the outer magnetic path to the length l_2 of the inner one (that is, $\gamma_r=l_1/l_2$) as shown in Fig.1(a).

When the core dimensions and the leg fluxes ϕ_u, ϕ_v and ϕ_w are given, the wave forms of respective magnetic flux densities can be obtained by solving non-linear simultaneous equations (1), (2) and (5). In the R3-type core, if the wave forms of the line voltages are symmetrical three-phase sinusoidal waves, the wave forms of the phase voltages applied to the legs are approximately symmetrical three-phase sinusoidal waves even in star connection; this can easily be proved. Hence, the voltage e_u impressed upon the leg-U can be denoted as follows.

$$e_u=E \sin \omega t \ . \tag{6}$$

Then, we obtain the following:

$$\left.\begin{aligned}
\phi_u&=2B\mathrm{leg} \sin(\omega t-\pi/2) \ , \\
\phi_v&=2B\mathrm{leg} \sin(\omega t+5\pi/6) \ , \\
\phi_w&=2B\mathrm{leg} \sin(\omega t+\pi/6) \ ,
\end{aligned}\right\} \tag{7}$$

where ϕ_u, ϕ_v and ϕ_w are the fluxes in the legs U,V and W, Bleg is an apparent maximum flux density passing through each leg and is given by

$$B\mathrm{leg}=E/(2\omega N) \ . \tag{8}$$

In Eq.(8), N is the number of turns per each leg. We call the Bleg the leg flux density.

3. Calculation of Flux Wave Forms

3.1 Non-linear numerical calculation by digital computer

If above mentioned parameter γ_r and the leg flux density Bleg are given, then we can calculate the wave forms of flux densities in respective magnetic paths by solving Eqs.(1), (2) and (5). For this, ωt in Eq.(7) is increased at a regular step, for example, of 1°. We find the maximum and effective values, form factor and distortion factor of each wave form, as well as the amplitudes and the positions of the minor loops (3). We resolve this wave form into harmonics, and obtain the amplitudes and the arguments of each harmonic component. Detailed solving procedures for the non-linear simultaneous equations (1), (2) and (5) are as follows.

Let us assume that the flux density b_1 in the outer magnetic path is known, then the flux densities b_2 and b_3 in the inner magnetic paths are calculated from Eqs.(7), (1) and (2). When the quality of core materials is determined, the function f(b) in Eq.(4) is given, and m of the next equation can be calculated.

$$m=\gamma_r f(b_1)+f(b_2)+f(b_3) \ . \tag{9}$$

If m is equal to zero, above assumed value of b_1 is true, because Eq.(5) is satisfied.

If assumed b_1 is greater than true value, the values of b_2 and b_3 are also greater than true values of b_2 and b_3, because b_2 and b_3 are calculated from Eqs.(1) and (2). In this case, m takes a positive value, because f(b) in Eq.(9) is a monotonically increasing function according to the magnetization characteristics (2). After all, if the calculated value of m is positive against a certain assumed value of b_1, we recalculate m after decreasing b_1 by Δb. Of cource, if m is negative, we have to recalculate m after increasing b_1 by Δb. We repeat this process until the sign of m is changed. When the sign is once changed, the true value b_{10} of b_1 exists between $b_1-\Delta b$ and b_1 or b_1 and $b_1+\Delta b$. Therefore, hereafter the changing step of b_1 can be reduced by one-half of Δb, i.e. $\Delta b=\Delta b/2$. We repeat this process until the accuracy of b_1 is satisfied (This convergence method is named the "bitwise chopping method"). In our calculations, when Δb becomes less than 0.01 gausses, we regard the value of b_1 as the true value. The initial value of Δb is set almost equal to 0.02 Bleg.

Since the magnetic circuit of the R3-type core is of symmetric structure, b_1 is equal to zero at $\omega t=120^\circ$. This fact is also understood from the results of the linear solution. Therefore, it is preferable to start the computation from $\omega t=120^\circ$, because the initial value of b_1 is known in advance.

In the subsequent computation steps of ωt, the initial value of b_1 is set equal to the true value of b_1 which has been obtained at the previous step. Further, the initial variation interval Δb is set equal to the difference between the initial and the true values of b_1 which have been obtained at the previous step.

ωt is varied at intervals of 1°. Taking the intervals of ωt too small, the computing times become many. On the contrary, taking it too large, the computed wave form becomes inaccurate and the time of convergence is prolonged, because the error of the initial value of b_1 becomes greater.

The computing intervals of ωt are sufficient between 120° and 210°. Since the magnetic circuit of the R3-type core is of symmetric structure, the values of b_1, b_2 and b_3 in the other intervals can be calculated by the following equations (2), (4), (5).

$$\left.\begin{aligned} b_1(\omega t)&=b_1(60^\circ-\omega t)=-b_1(240^\circ-\omega t)\ , \\ b_2(\omega t)&=b_3(60^\circ-\omega t)=-b_3(240^\circ-\omega t)\ , \\ b_3(\omega t)&=b_2(60^\circ-\omega t)=-b_2(240^\circ-\omega t)\ . \end{aligned}\right\} \qquad (10)$$

Considering the nature of the magnetization curve, all solutions of Eqs.(1), (2) and (5) are single roots. Therefore, when dm/db_1 is large, the computing time becomes short by adopting the Newton-Raphson iteration.

3.2 QUALITATIVE DISCUSSIONS

Since the impressed three-phase voltage is balanced and the core is symmetrical with respect to the axis of V leg, the wave forms of b_2 and b_3 are the "inversed waves with phase difference 30°" (4).

Similarly, the wave form of b_1 which passes across the V leg is the "symmetrical wave at 90°" (4).

On the basis of the above discussions, we can express respective flux densities as follows:

$$b_1=B_{11}\ \sin(\omega t-2\pi/3)+\Sigma B_{1n}\sin n(\omega t-2\pi/3)\ , \qquad (11)$$

$$\left.\begin{aligned} b_2 &= B_{21}\ \sin(\omega t+2\pi/3-\theta_{21})+\Sigma B_{1n}\sin\ n(\omega t-2\pi/3)\ , \\ b_3 &= B_{21}\ \sin(\omega t+\theta_{21})+\Sigma B_{1n}\sin\ n(\omega t-2\pi/3)\ , \end{aligned}\right\} \qquad (11)$$

where B_{1n} is the magnitude of the n-th harmonic, and is influenced by f(b) denoting the magnetization curve in Eq.(4). B_{21} and θ_{21} are given by the following equations:

$$\left.\begin{aligned} B_{21} &= \sqrt{B_{11}^2-2\sqrt{3}\ B_{11}B\mathrm{leg}+(2B\mathrm{leg})^2}\ , \\ \theta_{21} &= \tan^{-1}\{(2B\mathrm{leg}-\sqrt{3}B_{11})/(2\sqrt{3}B\mathrm{leg}-B_{11})\}\ . \end{aligned}\right\} \qquad (12)$$

Figure 3 shows the vector diagram of the distorted wave (4) at the moment $\omega t=0°$ in Eq.(11); the phase angle of the n-th harmonic vector is multiplied by a factor of 1/n in Fig.3. The phase angle of the fundamental vector B_{11} in the outer magnetic path is fixed constantly at -120°. The fundamental vectors $\dot{B}_{21}$ and $\dot{B}_{31}$ of the flux densities in the inner magnetic paths are symmetric with respect to the axis of which angle is identical with that of $\dot{B}_{11}$, i.e. -120°. When γ_r changes from 1 to infinity, θ_{21} varies from 0° to 30° inside the hatched extent. These facts are similar to θ in the case of linear solution. The phase angle of the n-th harmonic vector $\dot{B}_{1n}$ in the outer magnetic path is in- or anti-phase with the fundamental vector $\dot{B}_{11}$ in that path. Whether it is in- or anti-phase is determined by the flux density in the leg (i.e. the shapes of the magnetization curve). The higher harmonic in the inner magnetic paths are the same as B_{1n}.

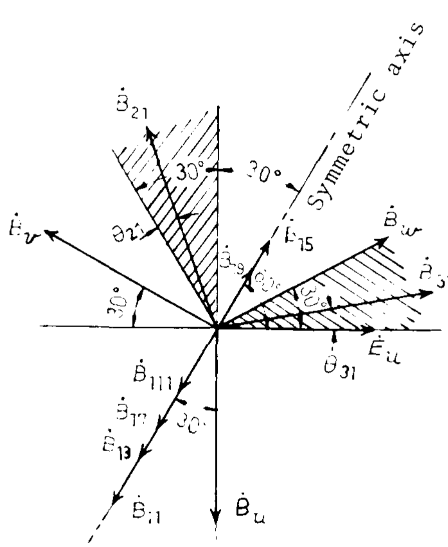

Fig.3 Vector diagram.

3.3 CALCULATED FLUX WAVE FORMS

In the numerical calculations, the leg flux densities are varied from non-saturated region to saturated region. Each figure in this Section represents the calculated results obtained from model transformers to be stated in Chapter 5. The core quality of the model transformers is S10 (Cold-rolled silicon steel strip: JIS C 2552-1970 (Grade: AISI-68 M-15)) and the core dimensions are designed by $\gamma_r=1.8$. Points designated by • in these figures denote the linear solutions (1) and those designated by × and ⊗ represent the measured values obtained from the model transformers. The reader is referred to Fig.3 for the meanings of amplitude B_{1n} and phase shift θ_{21}.

In the R3-type core, only the ratio γ_r has influences on the distribution of fluxes and the other dimensions have no influence.

In the case of a linear solution, if γ_r is decreased to 1, θ is also decreased to zero (1). This tendency is similar to θ_{21} in the case of non-linear solution. As the leg flux densities become high, γ_r affects little, and θ_{21} is nearly equal to zero independently of γ_r. This is because the magnetic resistances in respective magnetic paths tend to be balanced due to the core saturation. Hence, at the same flux densities, θ_{21} in the core which is made of non-grain-oriented silicon steel is smaller than that made of grain-oriented one.

If γ_r is equal to 1, $B_{11}=B_{21}=2Bleg/\sqrt{3}$. This is independent of the leg flux density, and B_{11} and B_{21} are the same as the linear solutions (1). Presuming from the linear solutions, the cause to $B_{11}<B_{21}$ as shown in Fig.4 is γ_r. In the same reason described above, the flux densities B_{11} and B_{21} are balanced in the high flux-density region, and both approach $2Bleg/\sqrt{3}$.

If the leg flux density becomes high, the contents of the third harmonic component are increased and saturated gradually as shown in Fig.4. This contents are the largest in all harmonics, and the value reaches upward 20% in the region of the leg flux density commonly used. The contents are hardly affected by the quality of the core material and the parameter γ_r.

If γ_r is equal to 1, the fifth and seventh harmonics cannot exist, because these harmonic fluxes are occured due to the unbalance of the magnetic resistances in respective magnetic paths. Hence, in the high flux-density region, these fluxes are negligible independently of γ_r. In a core having ordinary size, i.e. $\gamma_r=1.8$, the contents of the 5th or 7th harmonic are less than 1% and are smaller than those of the 9th harmonic (about 2%) at the flux density commonly used.

Increasing the leg flux density, the magnitudes of the fundamental harmonic vectors B_{11} and B_{21} approach $2Bleg/\sqrt{3}$. On the other hand, the maximum flux densities B_1 and B_2 in the outer and inner magnetic paths approach the leg flux density Bleg. (In the case of linear solution, the maximum flux densities are only the function of γ_r.) At low flux density, the maximum flux density B_1 in the outer path decreases with increasing γ_r, whereas the maximum flux densities B_2 and B_3 in the inner paths increase as well as the case of linear solutions.

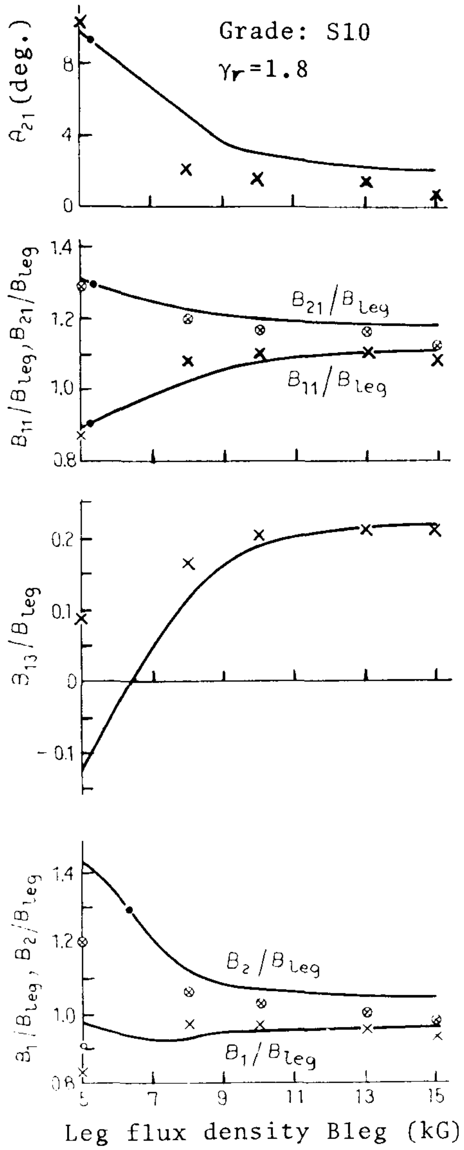

Fig.4 Analysed results of wave forms in each magnetic path.

Figure 5 shows the wave forms of flux densities b_1 and b_2 in the outer and inner magnetic paths with a parameter of the leg flux densities. Figure 5(a) shows the computed results using the solid lines, and the linear solutions (a sinusoidal wave) at 10 kG are shown by the dotted lines for comparison. Figure 5(b) shows the measured results. As the leg flux density becomes high, b_1, b_2 and b_3 tend to contain large amounts of the third harmonic which is mixed in-phase with the

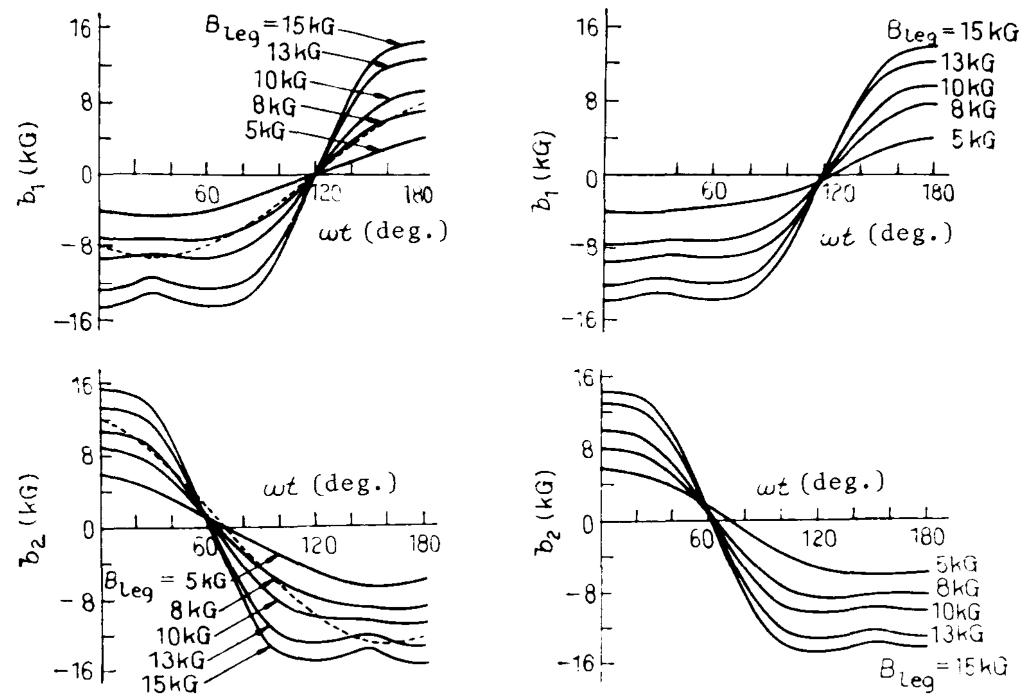

(a) Computed wave forms (b) Measured wave forms

Fig.5 Flux density wave forms in each magnetic path.

fundamental wave, the maximum value of the wave is depressed, and a cavity arises at the top of the wave form. It is caused by the minor loops in the hysteresis loop. The contents of minor loop in this figure are less than 5%.

If γ_r is equal to 1, b_1, b_2 and b_3 form exactly the same symmetrical distorted waves containing only the zero phase sequence components, and are the "symmetrical wave at 90°" respectively, because B_{11} is equal to B_{21} and θ_{21} is equal to zero. At high flux density, the wave forms are hardly affected by γ_r.

The wave form of b_1 is the "symmetrical wave at 90°" and crosses with the quadrature axis at $\omega t=120°$. The wave forms of b_3 are omitted, because b_2 and b_3 are symmetric with respect to the axis of $\omega t=30°$. As the phase angle of the fundamental wave is shifted by θ_{21} from symmetrical position as shown in Fig.3, the second peak value of b_2 is higher than the first one. With decreasing leg flux density, the value of ωt at the point, on which b_2 crosses with the quadrature axis, increases from 60°. The cause of this phenomenon is also due to the increasing θ_{21}. Hence, the similar tendency occurs when γ_r increases.

The form factor of b_1 is greater than those of b_2 and b_3, and this tendency becomes remarkable as γ_r increases. The reason is as follows:

As was stated above, the contents of the third harmonics in each magnetic path are the same with each other, and they are hardly affected by γ_r. On the other hand, the B_{21} is greater than the B_{11} as shown in Fig.4 and this tendency is remarkable when γ_r increases.

With increasing leg flux density, the form factors of the respective wave forms increase.

4. DISCUSSIONS ON CORE LOSSES

Since the maximum flux density Bm, the effective flux density Be and the amplitude Bk (3) of the minor loop have been determined, we can now calculate the core losses using the method proposed in reference (3) as follows (1):

$$Wh=[\gamma_r\{w_h(B_1)+2\Sigma w_h(Bk_1)\}+2\{w_h(B_2)+2\Sigma w_h(Bk_2)\}]/(\gamma_r+2)\ , \qquad (13)$$

$$We=\{\gamma_r w_e(Be_1)+2w_e(Be_2)\}/(\gamma_r+2)\ , \qquad (14)$$

where Wh is hysteresis loss (W/kg), We is eddy current loss (W/kg), w_h(Bm) is the hysteresis loss (W/kg) produced by maximum flux density Bm, and w_e(Be) is the eddy current loss produced by flux density Be. Be is given by the following equation.

$$Be=\sqrt{\Sigma(nBn)^2}=2\sqrt{2}FBm/\pi\ , \qquad (15)$$

where Bn represents the amplitude of the n-th harmonic flux density, and F is the form factor of this wave.

Now, σ, σ_h and σ_e defined by

$$\left.\begin{aligned}\sigma&=(Wh+We)/\{w_h(Bleg)+w_e(Bleg)\}\ ,\\ \sigma_h&=Wh/w_h(Bleg)\ ,\\ \sigma_e&=We/w_e(Bleg)\ ,\end{aligned}\right\} \qquad (16)$$

represent the total core-loss ratio, hysteresis loss ratio and eddy current loss ratio, respectively, of the R3-type core to the B-type core. Figure 6 shows 60Hz core-loss ratio σ in the model transformers to be stated in the Chapter 5. The solid line in Fig.6 represents the calculated curve, and the dotted line and the chain line represent the measured curves. The function forms of w_h and w_e have been determined from the results of the Epstein tester using parallel specimens by the distorted wave method described in reference (3). In this sense, σ, σ_h and σ_e represent the core-loss ratios based on the Epstein loss. Generally, the core losses of the B-type core are a little greater than that of Epstein tester. The fact that in Fig.6, the chain line lies above the dotted line is explained by this phenomenon.

At usual operating leg flux density, σ is hardly affected by γ_r, and this is caused by the balancing act of magnetic resistances due to the saturation of the magnetic paths. With increasing frequency, σ increases, because the eddy current loss is increased due to the harmonic fluxes. From the same reason, the

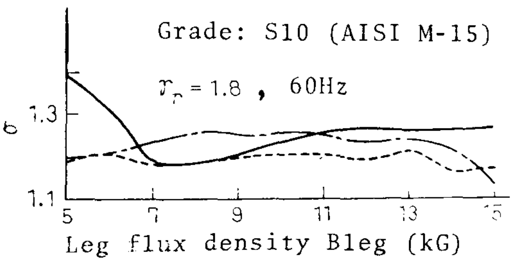

Solid line: calculated core-loss ratio
Dotted line: measured core-loss ratio based on the sum of core losses, each of which is measured independently in each magnetic path
Chain line: measured core-loss ratio based on Epstein loss

Fig.6 Relations between the flux density in the leg and core-loss ratios of the model transformer.

increased core losses are remarkable in such core materials as grain-oriented silicon steel where the eddy current loss is considerably large. The principal causes to increase the eddy current loss are the fluxes of the third and ninth harmonics.

5. Experimental Studies Based on Model Transformers

5.1 Model transformers and experimental methods

Three cores having the same dimensions commonly used are constructed as models. One is the wound strip core made of grain-oriented silicon steel G10 (Grade: AISI-68 M-5). Another two cores are the stacked cores made of non-grain-oriented silicon steel, and the qualities of the core materials are S10 (Grade: AISI-68 M-15) and S09F (Grade: AISI-68 M-14) respectively. The dimensions, the winding arrangement and the connections are the same as the case of the R6-type core (2).

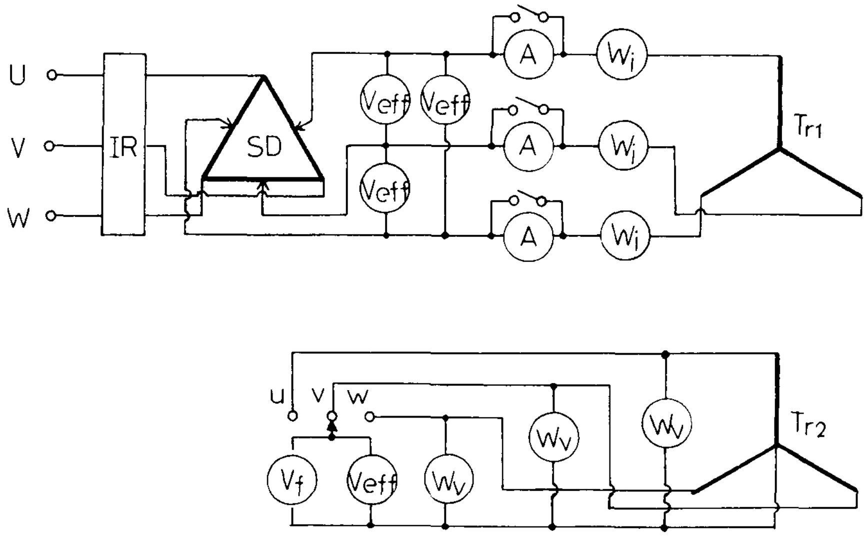

Tr1, Tr2: 1st and 2nd windings of the model transformer
IR: Three phase induction regulator
SD: Single phase autotransformer
Veff: RMS voltmeter
Vf: Flux voltmeter
Wi: Current coil of watt-meter
Wv: Potential coil of watt-meter
A: High frequency RMS ammeter

Fig.7 Measuring circuit of core losses.

Figure 7 shows the measuring circuit of core losses. The commercial power source of 60Hz and 200V is used as a power source. The induction regulator IR of 3kV and 1600kVA is connected and we have tried to obtain a stabilized voltage having little distortion of the wave forms. The applied voltages of each leg are regulated by the autotransformers SD. Both primary and secondary windings and the potential coils of watt-meters are all connected in star. The distortions of the applied voltage wave forms are less than the case of the delta connection, because the line current is smaller than that of the delta connection. The distortions of the phase (line-to-neutral) voltages due to the absence of stabilizing delta windings are negligible.

The core losses are measured by the three-watt-meter methods. At very high flux density, the indication of the watt-meter of the U-phase becomes negative. In such a case, an algebraic sum obtained from the reading three watt-meters must be used to be the three phase losses. The core losses have been measured in the flux density range between 5 and 15kG at intervals of 1kG. The induced voltage wave forms have been measured at 5, 8, 10, 13 and 15kG.

5.2 MEASURED RESULTS AND DISCUSSIONS

In this Section, only the experimental results for the core made of S10 are explained. Figure 5(b) shows the measured wave forms of the flux densities in each magnetic path. Their harmonic amplitudes and phase angles and their maximum values have been already represented in Fig.4 (see points denoted by x and ⊗).

The measured wave forms agree very well with calculated ones in the medium leg flux-density region. To study the causes of the disagreement except for the medium leg flux-density region, we discuss about the assumptions used in analysis and the accuracy of experimental results.

(1) Transfer of the fluxes across the magnetic paths. The amount of the fluxes crossing a cooling duct is a function of the difference of the flux densities between the neighboring two magnetic paths. Moreover, the width δ of the duct and its opposite area may be concerned. The detailed discussions for this problem will be reported later. At high leg flux density, there is a considerable amount of fluxes crossing the cooling duct and it may cause an error. Because of the magnetic flux crossing the cooling duct, the difference of the first and second peak values of the measured wave form of b_2 is not remarkable than that of the calculated one.

(2) Magnetization curve. Though we have taken the so-called magnetization curve for the function f(b) in Eq.(4), it seems to be preferable that the curve joining the centres of the hysteresis loop is used to be the function f(b) determing the flux distribution. In Fig.8, the solid line Lm denotes the magnetization curve, and the dotted line Lo shows the curve joining the centres of the hysteresis loop Li. The principal difference between them is the following:

The derivative of the curve Lo is a monotonically decreasing function. On the other hand, a derivative of the curve Lm is a increasing function at low flux density. Though the curve Lm consists of only one curve, the curves Lo exist infinitely, present various forms according to the maximum flux densities and exist above the curve Lm.

It is impossible to express the curves Lo as a function of only instantaneous value of flux density like Eq.(4), because the curve Lo varies depending on the maximum flux density. On the other hand, the maximum flux density cannot be obtained unless the form of this function f(b) has been given. From these reasons, the magnetization curve commonly used is employed as the function f(b) to calculate the flux distribution.

To discuss the influence of the slope of the curve f(b), the wave forms are also computed using the curve Lo which is obtained when the maximum flux density is equal to 12kG. In Fig.4, the third harmonic vector is anti-phase with the fundamental one at low flux density. The results of this time show that the third harmonic is in-phase with the fundamental one in all the intervals of the flux density as same as the experimental results. Hence, the abnormally increasing B_1/Bleg and B_2/Bleg at low flux density disappears and B_1/Bleg shows a monotonically increasing characteristics as well as the experimental results. On the contrary to the wave forms in Fig.5(a), the wave shapes computed here at 5kG are similarly depressed to the experimental results. On the other hand, θ_{21} decreases and is less than 6° at 5kG. The difference between "B_{21}" and "B_{11}" decreases at low flux density. When the leg flux density becomes over 10kG, the shapes of the magnetization curve will have hardly influence on the wave forms.

After all, it may be concluded that the slope of the magnetization curve must be decreased monotonically. We are now continuing this study.

(3) Core losses. With increasing leg flux density Bleg, the maximum flux densities B_1, B_2 and B_3 in each magnetic path approach "Bleg" as shown in the Section 3.3, and the effective flux densities Be in each path approach 1.4Bleg. Hence, for example, if "Bleg" is equal to 14kG, "Be" takes about 20kG. However, as the measurement of the core losses at high flux density is extremely difficult, it is presumed to include a certain error in the core-loss curve "w_e" in Eq.(14). Accordingly, the core-loss ratio will also have a certain error in the high flux-density region. It may be explained from this reason that the curve of chain line in Fig.6 descends in the high flux-density region. The measuring method of core losses at high flux density will be detailed elsewhere.

The calculating method of the core losses produced by the distorted wave, which is proposed in Eqs.(18) and (19), may also have a few errors (3). But it will have hardly influence on the core losses, because the contents of minor loop are small as described above.

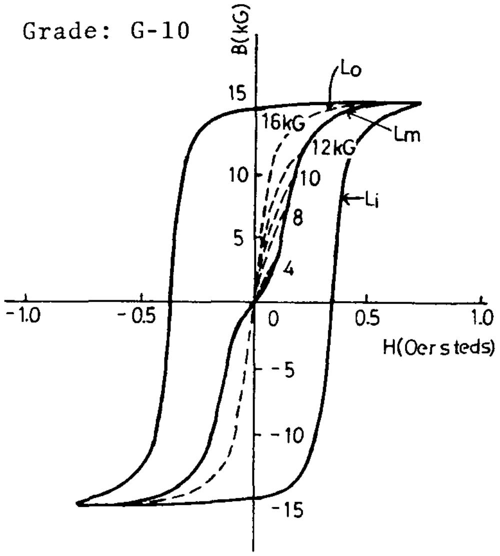

Lm: Magnetization curve
Li: Dynamic hysteresis loop
Lo: Curves joining the centre of the hysteresis loops

Fig.8 Magnetization curves and dynamic hysteresis loop at 50Hz.

(4) Phase angles of harmonic vectors. The phase angles of individual harmonics have been obtained from the next procedures. The voltage wave form recorded on a x-y recorder is read at intervals of 15°, and these read data are put into an electronic computer and we perform the harmonic analysis. Hence, in addition to the error corresponded to the ability of the x-y recorder, the error of a few degrees due to the reading may arise. This problem will be solved using the measuring instrument which is equipped with digital output terminals and is directly connected with the computer.

Besides the primary factors of the error mentioned above, the influence of the wave form distortion of power source is not negligible at high flux density.

6. Conclusions

The flux distributions in the transformer core of double-layer consisted of three independent magnetic paths have been analysed numerically considering the non-linearity and the magnetic path-length ratio. From the analysed results, the core losses have been also calculated. To confirm the validity of these theoretical analysis, an experimental investigation was performed using a few model transformers. We have obtained clear-cut results to solve the problem.

These results are summarized as follows:

(1) The magnetic characteristics of the R3-type core are only influenced by the magnetic path-length ratio γ_r related to dimensions.

(2) The flux wave form in the outer magnetic path is the "symmetrical wave at 90°", and the phase angles of the harmonic vectors are constant independently of core dimensions.

(3) The flux wave forms in the inner two magnetic paths are the "inversed waves with phase difference 30°". The amplitudes and phase angles of the higher harmonics are exactly the same as those in the outer magnetic path.

(4) In the leg flux-density region above the usually used region, all the wave forms tend to contain considerable amounts of the third harmonic component which depress the wave form and cause the minor loops.

(5) In the low flux-density region, the flux densities in respective magnetic paths tend to be more unbalanced as γ_r increases. In the high flux-density region, however, γ_r affects hardly the magnetic characteristics, and the magnetic flux densities in all magnetic paths are all balanced and approach the leg flux density. This is because the magnetic resistances in respective magnetic paths tend to be balanced due to the core saturation.

(6) The core losses of the R3-type core are larger than those of the Epstein tester. The increasing ratio in the leg flux density usually used attains to 20 to 30% in a core made of non-grain-oriented silicon steel and 40 to 60% in a core made of grain-oriented one.

(7) The core losses of the R3-type core are larger than those of the B-type core, because the eddy current loss is increased in the former due to the higher harmonic fluxes. Therefore, the core losses become large in such core material as grain-oriented silicon steel or in such a case when the frequency of the power source is high.

(8) The flux distributions and core losses are greatly affected by the shapes of the magnetization curve and the core-loss curve, i.e. the quality of the core material. Hence, the linear solutions are fairly different from the experimental results.

(9) As the function form of the B-H curve determining the flux distributions, the curve joining the centre of the hysteresis loop should be used instead of the so-called magnetization curve. However, at high leg flux density, the shapes of the magnetization curve are hardly affected.

REFERENCES

(1) T.Nakata and Y.Ishihara: Memoirs School Eng., Okayama Univ., 6 (1971), 67-82.

(2) T.Nakata, Y.Ishihara and M.Nakano: Electrical Engineering in Japan, 91 (1971) No.3, 17-28.

(3) T.Nakata, Y.Ishihara and M.Nakano: Ibid., 90 (1970) No.1, 10-20.

(4) T.Nakata and Y.Ishihara: Memoirs School Eng., Okayama Univ., 7 (1972), 85-88.

(5) T.Nakata and Y.Ishihara: Jour.I.E.E., Japan, 92-A (1972), 241-245.

(6) T.Nakata: 1972 National Conv. of Elec. Engrs., Japan, Symposium S.6-2(i).